Malays. J. Anal. Sci. Volume 30 Number 5 (2026): 1887

MALAYSIAN JOURNAL OF ANALYTICAL SCIENCES

Journal homepage: https://mjas.analis.com.my/

Research Article

Response surface methodology assisted electrochemical sensor for the detection of 3-MCPD

Mohd Zaheer Khan Mohd Ali[1], Wan Jefrey Basirun[2], Zainiharyati Mohd Zain[3], Siti Nor Atika Baharin[1], Mohd Azerulazree Jamilan[4], and Kavirajaa Pandian Sambasevam[1,3*]

[1]Advanced Materials for Environmental Remediation (AMER), Faculty of Applied Sciences, Universiti Teknologi MARA, Cawangan Negeri Sembilan, Kampus Kuala Pilah, 72000, Kuala Pilah, Negeri Sembilan, Malaysia
[2]Department of Chemistry, Faculty of Science, Universiti Malaya, 50603, Kuala Lumpur, Malaysia.
[3]Electrochemical Material and Sensor (EMaS) Research Group, Universiti Teknologi MARA, Shah Alam, 40450 Selangor Malaysia
[4] Nutrition Unit, Nutrition, Metabolism and Cardiovascular Research Centre (NMCRC), Institute for Medical Research, National Institute of Health, Ministry of Health Malaysia, No. 1, Jalan Setia Murni U13/52, Setia Alam, 40170 Shah Alam, Selangor D.E., Malaysia

*Corresponding author: kavirajaa@uitm.edu.my

Received: 1 April 2026; Revised: 12 June 2026; Accepted: 24 June 2026; Published: 31 October 2026

Abstract

3-MCPD (3-monochloropropane-1,2-diol) is a chemical contaminant formed during high-heat food processing. It is mostly found in refined vegetable oils (especially palm oil) and soy sauce. It is a suspected human carcinogen and has been linked to kidney damage. Because of these severe health risks, global food safety authorities strictly regulate and monitor its levels to ensure public safety. A molecularly imprinted polypyrrole/chitosan (MIPPy/CHT) electrochemical sensor was fabricated via electropolymerization for the selective detection of 3-monochloropropane-1,2-diol (3-MCPD). The surface morphology and elemental composition were characterized using field emission scanning electron microscopy (FESEM) coupled with energy-dispersive X-ray spectroscopy (EDX), while electrochemical techniques were employed to evaluate interfacial behavior and sensing performance. Fabrication parameters were systematically optimized using Response Surface Methodology (RSM). A two-level factorial design identified pH, number of scans, starting potential, and elution time as influential factors, with pronounced quadratic effects observed for pH, scan number, and starting potential. Mildly acidic conditions (pH 4) enhanced hydrogen-bonding interactions, while excessive number of scans and higher starting potentials for sensor fabrication reduced sensor response(A). Subsequent optimization using a Box–Behnken design (BBD) established optimal conditions at pH 4, 3 electropolymerization scans, lower electropolymerization starting potential at 0V, and 15 min elution time. Significant interaction effects were observed between pH and scan number, as well as between scan number and starting potential, confirming the critical balance between polymer growth and cavity accessibility. Under optimized conditions, the sensor exhibited a linear response toward 3-MCPD over 100–500 nM with a high correlation coefficient ($R^2 = 0.9963$). The limit of detection (LOD) and limit of quantification (LOQ) were 36 nM and 111 nM, respectively. These results demonstrate that the MIPPy/CHT sensor provides high sensitivity, good selectivity, and reliable analytical performance for 3-MCPD detection.

Keywords: 3-monochloropropane-1,2-diol, molecularly imprinted polymer, polypyrrole/chitosan composite, electrochemical sensor, response surface methodology

Introduction

3-Chloro-1,2-propanediol (3-MCPD) is a process contaminant formed during high-temperature refining of fats and oils, leading to its presence in products such as soy sauces and refined edible oils [1]. 3-MCPD has raised significant safety concerns due to documented nephrotoxic, reproductive, and carcinogenic effects observed in experimental studies, with kidneys and testis identified as primary target organs on rodents [2, 3]. Based on toxicological evidence, the International Agency for Research on Cancer has classified 3-MCPD as a Group 2B compound (possibly carcinogenic to humans) [4]. The European Commission's Scientific Committee for Food derived a Tolerable Daily Intake (TDI) of 2 µg/kg body weight for 3-MCPD. The figure of 2 µg/kg body weight is the same as the Provisional

Maximum Tolerable Daily Intake (PMTDI) established by the Joint FAO/WHO Expert Committee on Food Additives (JECFA) [5]. Given its adverse health implications and regulatory constraints, the development of rapid, sensitive, and reliable analytical methods for trace-level determination of 3-MCPD is essential; however, direct analysis is challenging due to the absence of a strong chromophore, largely making it inactive for conventional optical detection methods such as UV–Visible spectroscopy. 3-MCPD molecules also lack electro-active or redox-functional groups which makes it difficult to produce a detectable electrochemical signal within typical potential ranges. As a result, derivatization and advanced chromatographic methods are needed for accurate and sensitive measurement [6].

Conventional analytical methodologies including gas chromatography (GC), gas chromatography–mass spectrometry (GC–MS), and high-performance liquid chromatography (HPLC) have been widely applied as standard approaches for 3-MCPD quantification [6]. While these techniques provide high sensitivity and structural confirmation, they are typically associated with labor-intensive sample pretreatment, multistep derivatization procedures, high solvent and reagent consumption, costly instrumentation, extended analysis time, and the requirement for specialized technical expertise. These limitations reduce their practicality for rapid screening, real-time monitoring, or large-scale routine food safety control, particularly in complex matrices such as soy sauce and edible oils.

In response to these constraints, molecularly imprinted polymer (MIP)-based sensing platforms have gained increasing attention as selective, robust, and economically viable alternatives. MIPs are synthetic recognition materials fabricated by polymerizing functional monomers in the presence of a template molecule, followed by template removal to generate binding cavities complementary in size, geometry, and chemical functionality to the target analyte [7]. For 3-MCPD detection, functional monomers such as p-aminothiophenol (p-ATP) [8] have been employed, exploiting hydrogen bonding interactions between the amino groups of the monomer and hydroxyl groups of 3-MCPD during pre-polymerization assembly. To further enhance analytical performance, numerous nanostructured materials and conductive substrates have been incorporated into MIP-based electrochemical sensors to increase surface area, improve charge transfer efficiency, and amplify signal response. Gold nanoparticles (AuNPs) have been electrodeposited onto glassy carbon electrodes (GCE) to provide abundant reactive sites, high conductivity, catalytic activity, and enlarged effective surface area for increased imprinting density [9]. Nanoporous gold (NPG), characterized by its uniform porous morphology and outstanding electrocatalytic properties, has been coated onto GCE surfaces to support stable MIP membrane growth and facilitate efficient mass transport [10]. Prussian blue (PB), possessing a unique electroactive metal–chelate framework capable of reversible multi-electron transfer, has been used as an electron mediator to enhance signal transduction [11]. Graphene oxide (GO) has also been introduced to increase conductivity and surface roughness, particularly in molecularly imprinted polymer overoxidized polypyrrole on graphene oxide MIP(oPPy)-GO impedimetric platforms [12]. Electro-deposition strategies have therefore been employed to increase its specific surface area and provide additional active sites for MIP formation. Advanced sensor configurations reported include MIP/AuNP/GCE, MIP/NPG/GCE, MIP/Pt@PB/EM-GP, and MIP(oPPy)-GO modified disposable graphite electrodes, each demonstrating improved analytical characteristics through synergistic integration of nanomaterials and molecular imprinting.

Polypyrrole (PPy) is a conducting polymer utilized as a molecularly imprinted polymer (MIP) in electrochemical sensors because of its distinctive characteristics. Its intrinsic conductivity, environmental resilience, and straightforward production via electropolymerization make it an optimal choice for sensor applications [13]. Molecular imprinting utilizes PPy as a stable matrix to create cavities which permit selective rebinding of the analyte, hence enhancing its detection in intricate sample matrices. Moreover, PPy is compatible with diverse electrode materials and its ability to create homogeneous, thin films improve sensor performance, rendering it a suitable candidate for the advancement of next-generation electrochemical sensors [14]. Chitosan (CHT) has been widely studied due to its high adsorption potential. The abundant hydroxyl and amino groups on the chitosan surface provide an excellent platform for chemical modifications to enhance its adsorption performance. CHT's excellent thin filming ability makes it an ideal material to be used for the polymer-based sensor [15]. By combining PPy and chitosan, this hybrid material exhibits enhanced properties that make it ideal for high-performance electrochemical sensors. The synergistic interactions between these components could enable the development of low-cost, highly efficient, and selective electrochemical sensors for real-time monitoring of environmental contamination.

The Design of Experiments (DoE), particularly factorial design, provides significant advantages over the

conventional one-factor-at-a-time (OFAT) approach by enabling the simultaneous evaluation of multiple variables and their interactions in a structured and statistically robust manner. Unlike OFAT, which examines parameters individually and may overlook synergistic or antagonistic effects, DoE reduces the total number of experimental runs while conserving time and reagents and delivering more comprehensive insight into process behavior [16]. In this study, a two-level factorial design was first employed as a screening tool to efficiently identify the most influential factors and eliminate insignificant variables, thereby preventing unnecessary complexity in subsequent modeling. This preliminary step ensures that only statistically significant parameters are carried forward into advanced optimization, improving model accuracy and experimental efficiency. Following the screening phase, a Box–Behnken design (BBD) was applied to the selected significant factors to evaluate their quadratic and interaction effects in greater detail and to determine the true optimum conditions. BBD was chosen because it enables robust response surface modeling without requiring extreme experimental combinations, while maintaining a reduced number of experimental runs [17]. This two-step approach enhanced predictive reliability, sensitivity, and selectivity of the developed sensor for 3-MCPD detection. Furthermore, validation through real sample analyses in soy sauce and palm oil confirmed the practical applicability of the platform, demonstrating its cost-effectiveness, scalability, and strong potential for real-world environmental and consumer product monitoring.

Previous studies have reported highly diverse analytical performances for 3-MCPD detection. A molecularly imprinted polymer (MIP)-based gold nanoparticle (AuNP)-modified glassy carbon electrode achieved an exceptionally low limit of detection (LOD) of 3.8×10^{-18} mol L^{-1} (S/N = 3) [9]. However, this value is approximately 12 orders of magnitude lower than the established regulatory limits for 3-MCPD in food products where the ultratrace sensitivity is impractical for routine food safety applications. Fang et al. reported fluorescence-based molecularly imprinted paper platforms; however, the surface modification procedure involved labor-intensive and time-consuming fabrication steps [18]. Similarly, Xing and Cao employed capillary electrophoresis coupled with amperometric detection, obtaining an LOD of 1.2×10^{-6} mol L^{-1} [19]. Collectively, these findings highlight the ongoing need to enhance analytical sensitivity while maintaining simplicity, cost-effectiveness, and suitability for disposable, on-site electrochemical detection with minimal matrix interference.

In the present work, MIPPy/CHT (molecularly imprinted polypyrrole–chitosan) based electrochemical sensor provided a balanced and application-oriented analytical performance. Pyrrole ensures the formation of a conductive polypyrrole imprinted matrix, while chitosan (CHT) contributes abundant functional groups and enhanced film-forming capability, facilitating stable template–monomer interactions and improved mechanical integrity. The synergistic interaction between pyrrole and chitosan provided mechanical stability, increased surface functionality, and facilitated hydrogen bonding interactions with 3-MCPD. MIPPy/CHT sensor is a simple, cost-effective, and deployable electrochemical sensor which was fabricated without complex nanomaterial modification, biological catalysts, or labor-intensive fabrication procedures for sensitive detection of 3-MCPD. While some reported methods can achieve extremely low detection limits, these often exceed what is necessary for regulatory monitoring and may involve complex or time-consuming fabrication. In contrast, this current work focuses on achieving adequate sensitivity within relevant concentration ranges using a simpler and more accessible approach. These aspects distinguish the present work as a balanced and application-oriented alternative to existing methods for 3-MCPD detection.

Materials and Methods

Chitosan (MW=50,000-190,000 Da), Pyrrole (99.5%), Nitric acid (70%), glacial acetic acid (99%), potassium chloride (99%), potassium ferricyanide $K_3[Fe(CN)_6]$, potassium ferrocyanide $K4[Fe(CN)_6]$, 3-MCPD (98%), 2-MCPD (98%), and palmitic acid (99%) were procured from Sigma Aldrich. Britton–Robinson buffer solution (0.1 M, pH 5) was prepared by adjusting the mixture of acid solutions including 0.1 M acetic acid, 0.1 M boric acid, and 0.1 M phosphoric acid, titrated with 0.2 M sodium hydroxide solution. All the aforementioned chemicals were purchased from Sigma Aldrich Malaysia. For the screen printed carbon electrode (SPCE) by Metrohm Dropsens, the working and auxiliary electrode was coated by Carbon paste while the reference electrode was coated by Ag paste. The SPCEs (model DRP-C110-U75) were purchased from Metrohm Malaysia, and distilled water was used throughout the research. A typical redox solution was prepared comprising the mixture solution of 5mM potassium ferricyanide $K_3[Fe(CN)_6]$, 5mM potassium ferrocyanide $K4[Fe(CN)_6]$, and 0.1M potassium chloride which shall henceforth be denoted as [Fe(CN)6]3-/4-.

Instrumentation

Morphological characterization was examined with scanning electron microscopy (SEM) with Energy-dispersive X-ray (EDX) probe (SEM, Tescan-Czech

Republic). Electrochemical characterizations were carried out via cyclic voltammetry (CV) and all measurements were implemented with Autolab PGSTAT302N model potentiostat/galvanostat using the SPCE coated with the desired materials.

Preparation of MIPPy/CHT

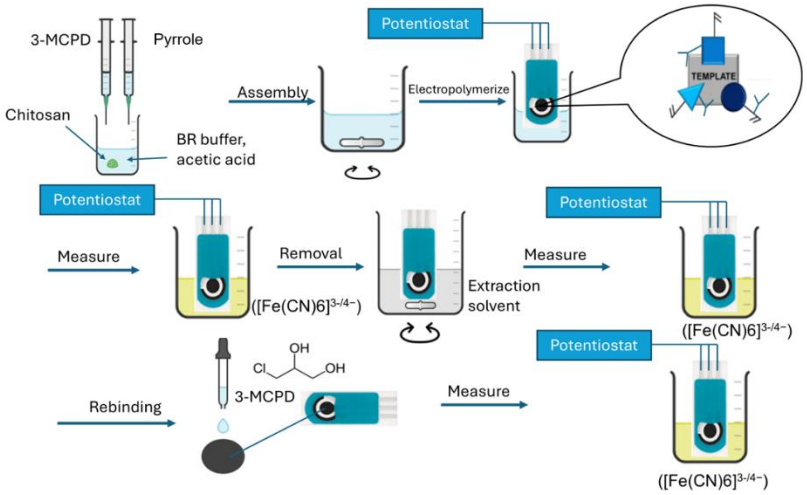
Electropolymerization was carried out using cyclic voltammetry based on a modified method [12]. Chitosan (0.019 g) was dissolved in 2 mL of 2% (v/v) acetic acid under constant stirring until a clear solution was obtained (denoted as CHT solution) [20]. Separately, a Britton–Robinson buffer containing 5 mM of 3-MCPD template and 10 mM Pyrrole monomer was prepared. The CHT solution was added to this mixture and stirred for 5 minutes to ensure homogeneity. The SPCE was then immersed in the solution, and electropolymerization was performed by cyclic voltammetry from 0.0 to +1.20 V at a scan rate of 100 mV/s for 3 cycles. Elution of the template molecule was carried out by immersing the modified SPCE in a 9:1 (v/v) methanol-water mixture which was stirred for 15 minutes and later rinsed using distilled water.

Electrochemical fabrication of MIPPy/CHT for 3-MCPD sensor

The electropolymerization of pyrrole-chitosan emulsion with the 3-MCPD molecules (5 mM as an optimum value) was carried out by cyclic voltametric in BR buffer pH 4.0 (as an optimum pH) in the potential range from 0.0–1.2 V on a readily available screen-printed electrode with 3 sweep cycles (as an optimum value) at 100 mVs-1, producing the molecularly imprinted polymer (MIP). Non-imprinted polypyrrole-chitosan (NIP) electropolymerization without 3-MCPD molecule was performed under the same conditions. The signal during 3-MCPD elution and rebinding of 3-MCPD of the MIP was compared using the [Fe(CN)6]3-/4- redox probe solution. The fabricated electrodes were washed to leach out 3-MCPD molecules from the MIP in 9:1 (v/v) methanol/water mixture for 15 minutes (as an optimum time). Developed electrodes were dried in an oven and stored at ambient temperature. Cyclic voltammetric (CV) characterizations were performed in redox probe solution (5.0 mM of Fe(CN6)3-/4- prepared in 0.1 M KCl) between -0.5 V to +1.1 V (vs. Ag/AgCl), at a scan rate of 100 mVs- 1 [21-23]. The analytical signal for 3-MCPD detection was calculated based on the relative change in peak current before and after rebinding of analyte using the following (Eq. 1) [24]:

$$Response = \frac{I_{eluted} - I_{rebinded}}{I_{eluted}} \quad (1)$$

This equation (Eq.1) is derived from the percentage change formula and represents the fraction of signal decrease upon analyte rebinding relative to the eluted MIP surface. Here, I_eluted corresponds to the peak current measured after template removal, when the imprinted cavities are vacant and electron transfer is maximized, whereas I_rebound represents the peak current after re-exposure to 3-MCPD, where cavity occupation partially blocks charge transfer. By normalizing the signal change to the eluted current, this approach minimizes electrode-to-electrode variation and emphasizes the specific binding effect of 3-MCPD within the imprinted sites. Consequently, the calculated response quantitatively reflects the degree of cavity occupation and provides a sensitive metric for evaluating sensor performance.



Scheme 1. Schematic Illustration of electrochemical fabrication of MIPPy/CHT and analysis of 3-MCPD

Optimization

Response Surface Methodology (RSM) incorporating a two-level factorial design was first applied to systematically evaluate the influence of critical fabrication and operational parameters on sensor performance [25]. The investigated factors included: (A) number of scans, which determines the thickness and density of the electropolymerized MIP layer; (B) pH, which affects monomer ionization, hydrogen bonding interactions, and overall polymer formation; (C) monomer-to-template (M:T) ratio, governing the formation and distribution of selective recognition cavities; (D) electropolymerization scan rate, influencing film uniformity and polymer growth kinetics; (E) starting potential, which controls the initiation of monomer oxidation and polymer nucleation; (F) elution time, determining the efficiency of template removal and accessibility of binding sites; and (G) rebinding time, affecting the equilibrium interaction between the analyte and the imprinted cavities [26-28]. Each variable was evaluated at two levels to screen as shown in **Table 1** for analysis of variance (ANOVA) to identify the most influential parameters.

The two-level factorial design was structured to explore the effect of each factor at two different levels: high and low. This type of experimental design allows for the identification of both the main effects and interactions between factors. The design matrix included various combinations of the factor levels, enabling a comprehensive analysis of the system under study [29]. The experimental setup involved performing a series of runs, each corresponding to a specific combination of factor levels. The response variable was measured in each run, and statistical tools were applied to analyze the relationship between the factors and the response. Based on the factorial screening results, the starting potential most statistically significant factors namely pH, elution time, and number of scans were selected for further optimization using a Box–Behnken design (BBD) [17, 30].

In this stage, each parameter was studied at three levels to evaluate their individual effects, quadratic behavior, and mutual interactions. Specifically, pH was optimized to balance polymer stability and effective hydrogen bonding interactions between the MIP matrix and 3-MCPD; elution time was refined to ensure complete template removal without damaging the imprinted cavities; and number of scans was adjusted to achieve an optimal polymer thickness that maximizes binding site density while preserving efficient mass transfer and electron communication. The BBD-generated response surface and contour plots enabled visualization of these combined effects and facilitated precise determination of the optimal operational conditions. This structured optimization approach enhanced model predictability, improved sensor performance, and ensured statistically reliable refinement of the critical fabrication parameters. Each variable was evaluated at three levels as shown in **Table 2** to determine the optimum parameters for the fabrication of MIPPy/CHT sensor.

The design matrix performed based on the RSM-BBD and their corresponding responses for 3-MCPD detection is reported in **Table 3**.

Table 1. Two level factorial design with low-high factors

Factor	Name	Low	High
A	Number of Scan	5	10
B	pH	4	5
C	M:T Ratio	2	4
D	Ep Scan rate	50	100
E	Starting potential	0	0.5
F	Elution time	10	15
G	Rebinding time	10	15

Table 2. Box-Behnken design low-medium-high factors

Factor	Name	Low	Medium	High
A	pH	4	5	6
B	Number of scan	3	6	9
C	Starting potential (V)	0	0.25	0.5
D	Elution time (min)	10	15	20

Table 3. Box-Behnken design variable matrix and experimental data

Run	A:pH	B:Number of Electropolymerization Scan	C:Starting Potential (V)	D:Elution Time (min)	Peak Current (A)
1	4	6	0.25	20	0.425
2	4	3	0.25	15	0.555
3	5	3	0	15	0.502
4	5	3	0.25	20	0.491
5	6	9	0.25	15	0.192
6	5	9	0	15	0.120
7	5	6	0.5	20	0.319
8	6	6	0	15	0.259
9	5	3	0.5	15	0.115
10	5	9	0.25	10	0.073
11	6	6	0.5	15	0.104
12	6	6	0.25	10	0.344
13	4	6	0.5	15	0.325
14	5	9	0.5	15	0.288
15	5	9	0.25	20	0.224
16	5	6	0	20	0.487
17	5	6	0.5	10	0.308
18	4	9	0.25	15	0.227
19	6	3	0.25	15	0.322
20	6	6	0.25	20	0.222
21	5	6	0	10	0.508
22	4	6	0	15	0.498
23	5	3	0.25	10	0.503
24	4	6	0.25	10	0.495

Characterization of MIPPy/CHT composite

The fabricated sensor bare SPCE, MIP-modified SPCE, eluted MIP, and rebound MIP were characterized using electrochemical analysis, field emission scanning electron microscopy with energy-dispersive X-ray spectroscopy (FESEM-EDX). EDX was utilized to detect residual chlorine atoms from 3-MCPD to confirm template incorporation and removal.

Real sample analysis

Real sample analysis was assessed by analyzing commercially obtained soy sauce and palm oil samples spiked with 3-MCPD to final concentrations of 150 nM (soy sauce) and 250 nM (palm oil), respectively. The soy sauce samples were spiked and kept in an ultrasonic bath for 10 minutes. The resulting sample was then extracted with 6 mL of dichloromethane. The sample was then transferred to a separating funnel containing 10 mL of water [31]. The lower aqueous layer was separated from the organic layer, which was re-extracted with another 10 mL portion of water. The fabricated electrodes were immersed into these solutions to rebind the 3-MCPD molecules. The palm oil samples were subjected to a liquid–liquid extraction using hexane/acetone. The samples were spiked with 3-MCPD and sonicated followed by a mixture of (1:1, v/v) hexane/acetone and stirred to homogenization. The mixture was then filtered using the Buchner funnel and the filtrate transferred to a separating funnel. The filtrates were washed with water multiple times followed by the drying of the organic layer to remove any remaining acetone. Finally, the extract was incubated with the prepared MIP electrode for analysis [11]. Recoveries were calculated as (measured concentration/spiked concentration) × 100% and precision reported as relative standard deviation (RSD).

Results and Discussion

Electrochemical characterisation of sensor via CV

Cyclic voltametric (CV) characterizations were performed in redox probe solution (5.0 mM of Fe(CN6)3- /4- prepared in 0.1 M KCl) between -0.5 V to +1.1 V (vs. Ag/AgCl), at a scan rate of 100 mVs- 1. As shown in **Figure 1**, the cyclic voltammograms of the MIP and NIP electrodes (color-coded as red: MIP before removal, green: MIP after template removal, blue: MIP after rebinding(rebound MIP), and black: NIP) exhibit a well-defined redox couple with an oxidation peak at approximately +0.35 – +0.45 V and a corresponding reduction peak at about −0.30 to −0.40 V. For the MIP before 3-MCPD template removal (red curve), a moderate redox current is observed because the template molecules remain embedded within the polymer matrix, partially blocking the imprinted sites and restricting efficient electron transfer. After elution (green curve), a significant increase in peak current is observed due to the successful removal of the 3-MCPD molecules, which creates cavities that enhance surface accessibility, facilitate diffusion of the redox probe, and decrease charge-transfer resistance. Upon rebinding of the target molecule (blue curve), the peak current decreases again because the analyte reoccupies the imprinted cavities, hindering electron transfer at the electrode–electrolyte interface [32-34]. The reappearance and enhancement of the redox signal after elution therefore confirm the reversible binding mechanism and successful formation of functional imprinted sites. In contrast, the NIP (black curve) exhibits a lower and less responsive redox current due to the absence of specific recognition cavities, indicating that the pronounced signal variation observed for the MIP arises from specific imprinting effects rather than non-specific adsorption.

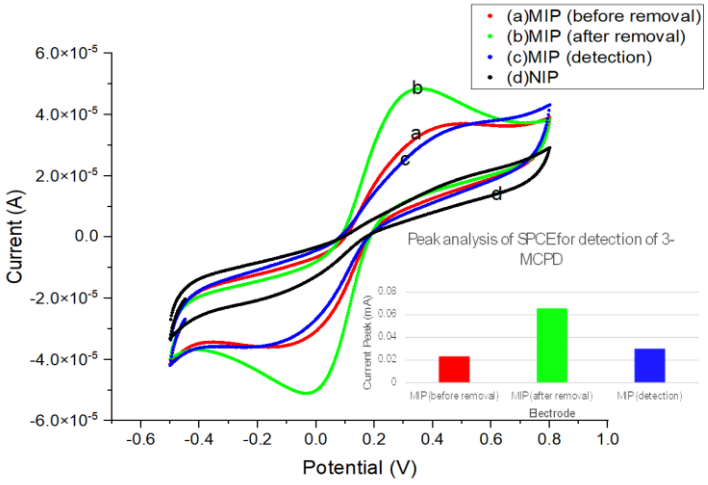


Figure 1. Cyclic voltammograms of MIPPy of different stages and NIP in redox probe solution

Optimization

A Response Surface Methodology (RSM) two-level factorial design was conducted to investigate the influence of various factors on the electrochemical detection of 3-MCPD. The factors included in the model were (A) Number of Scans, (B) pH, (C) M:T Ratio (Monomer-to-Template ratio), (D) Electro-polymerization scan rate, (E) Starting Potential, (F) Elution Time, and (G) Rebinding Time. The goal of this experiment was to determine which of these factors would significantly affect the response of the process. The two-level factorial design was structured to explore the effect of each factor at two different levels: high and low.

The results of the experiments are shown in **Figure 2** and **Table 4.** The data were analyzed using standard statistical techniques for RSM, including analysis of variance (ANOVA). The results of the analysis indicated the following:

- Factor A (Number of Scans): This factor was found to be statistically significant. The changes in the number of scans led to a noticeable variation in the response variable, suggesting its strong influence on the outcome of the process. With differences in the number of scans, the formation and stabilization of the imprinted polymer film on the electrode surface was altered, directly influencing the availability and accessibility of recognition sites for 3-MCPD binding.
- Factor B (pH): pH also emerged as a significant factor. Variations in pH levels significantly impacted the response, demonstrating the importance of pH control in the process. The pH directly influenced both the ionization state of the functional groups within the imprinted polymer and the interaction strength between the MIP cavities and 3-MCPD molecules [35]. Variations in pH changed the peak current response by modifying hydrogen bonding, electrostatic interactions, and charge-transfer kinetics at the electrode interface [36]. At non-optimal pH conditions, weakened binding interactions or reduced electron transfer efficiency led to diminished redox signals, whereas the optimal pH provided maximum peak current and binding stability
- Factor E (Starting potential of electropolymerization): The electropolymer-ization potential range was found to be statistically significant. The potential range showed that the greater the range, the higher the stability of the MIP. A broader potential range promoted more complete polymer growth and stronger anchoring of the film, which in turn preserved the fidelity of the 3-MCPD recognition cavities after template removal.
- Factor F (Elution Time): Elution time was identified as another significant factor. Changes in elution time showed a clear effect on the response variable. Insufficient elution time resulted in incomplete removal of 3-MCPD from the imprinted cavities, leading to partial blockage of active sites and reduced electron transfer. In contrast, optimized elution time ensured effective template removal, restored cavity accessibility, and maximized the oxidation/reduction peak current, thereby improving the sensitivity and reproducibility of subsequent 3-MCPD measurements.

As presented in **Table 4**, the two-level factorial design revealed that the overall regression model was statistically significant ($p = 0.0084$), indicating that the selected experimental factors collectively influenced the electrochemical response of the 3-MCPD MIP sensor. The model F-value of 15.88 further confirms the adequacy of the model, with only a 0.84% probability that such a large F-value could arise from random experimental noise. Among the factors investigated, the number of scans (A, $p = 0.0057$), pH (B, $p = 0.0082$), starting potential (E, $p = 0.0355$), and elution time (F, $p = 0.0115$) exhibited statistically significant effects ($p < 0.05$) on the redox peak current response associated with 3-MCPD detection. In contrast, the monomer-to-template (M:T) ratio (C, $p = 0.1834$), electropolymerization scan rate (D, $p = 0.1514$), and rebinding time (G, $p = 0.4249$) did not show significant contributions within the studied range ($p > 0.05$), suggesting that their influence on the sensor response was comparatively minor under these conditions. Figure 2 shows the Pareto chart of standardized effects obtained from the two-level factorial design for the optimization of the 3-MCPD MIP sensor. The vertical bars represent the absolute t-values of the main factors and their interactions, while the horizontal lines indicate the t-value significance limit (2.776) and the Bonferroni limit (6.254). Overall, the Pareto analysis highlights scan number, pH, elution time, and starting potential as the dominant factors governing the electrochemical performance of the MIP sensor for 3-MCPD detection. Therefore, these four significant factors were elected or further optimization.

Table 4. Analysis of variance (ANOVA) of each factors in the two-level factorial design

Source	Sum of Squares	df	Mean Square	F-value	p-value	Remarks
Model	0.7414	11	0.0674	15.88	0.0084	significant
A-Number of Scan	0.1237	1	0.1237	29.15	0.0057	significant
B-pH	0.1008	1	0.1008	23.75	0.0082	significant
C-M:T Ratio	0.0110	1	0.0110	2.58	0.1834	
D-Ep Scan rate	0.0133	1	0.0133	3.13	0.1514	
E-Starting potential	0.0413	1	0.0413	9.74	0.0355	significant
F-Elution time	0.0831	1	0.0831	19.57	0.0115	significant
G-Rebinding time	0.0033	1	0.0033	0.7878	0.4249	
AB	0.0391	1	0.0391	9.21	0.0386	significant
AD	0.0288	1	0.0288	6.78	0.0598	
AF	0.2111	1	0.2111	49.75	0.0021	significant
AG	0.0859	1	0.0859	20.24	0.0108	significant
Residual	0.0170	4	0.0042			
Cor Total	0.7584	15				

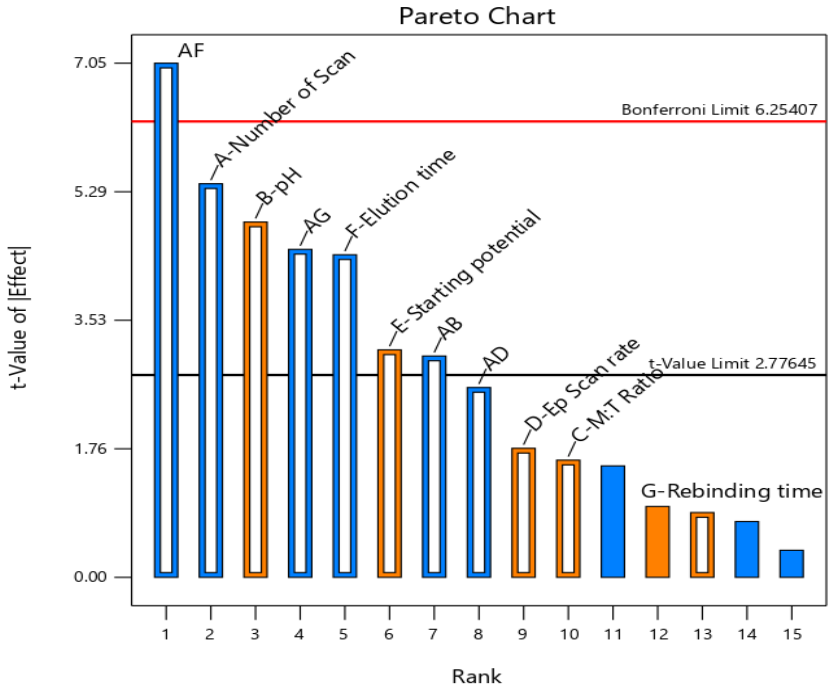


Figure 2. Pareto chart of the two-level factorial experimental model

The two-level factorial design revealed four significant factors influencing the MIPPy/CHT sensor, which were subsequently selected for further optimization using the Box–Behnken design (BBD). BBD was employed at this stage because it is an efficient response surface methodology capable of modeling quadratic effects and interactions among multiple variables [37]. Moreover, BBD reduces the number of experimental runs compared to other second-order designs while providing sufficient data to construct a reliable predictive model and accurately determine optimal parameter settings.

Table 5. ANOVA table of Box-Behnken experimental design

Source	Sum of Squares	df	Mean Square	F-value	p-value	remarks
Model	0.4211	13	0.0324	28.50	< 0.0001	significant
A-pH	0.0985	1	0.0985	86.68	< 0.0001	significant
B-Number of electropolymerization scan	0.0562	1	0.0562	49.41	0.0002	significant
C-Starting potential	0.0802	1	0.0802	70.61	< 0.0001	significant
D-Elution time	0.0083	1	0.0083	7.29	0.0306	significant
AB	0.0151	1	0.0151	13.27	0.0083	significant
AC	0.0001	1	0.0001	0.0772	0.7892	
AD	0.0007	1	0.0007	0.5836	0.4699	
BC	0.0791	1	0.0791	69.61	< 0.0001	significant
BD	0.0022	1	0.0022	1.97	0.2035	
CD	0.0002	1	0.0002	0.2178	0.6549	
A^2	0.0318	1	0.0318	27.96	0.0011	significant
B^2	0.0235	1	0.0235	20.65	0.0027	significant
C^2	0.0210	1	0.0210	18.50	0.0036	significant
D^2	0.0000	0				
Residual	0.0080	7	0.0011			
Cor Total	0.4291	20				

$$Response\ (A) = 0.48\ -0.10\ A\ -0.09B\ -0.09\ C - 0.03D + 0.08AB + 0.18BC - 0.10A^2 - 0.09B^2 - 0.08C^2 \qquad (2)$$

Significance via analysis of variance (ANOVA) is reported in Table 5. The p-value and F-value determined the relevance of the quadratic model for the response in this investigation. A model term is considered significant if it has a p-value <0.05 and a high F-value [38]. According to the ANOVA results in **Table 5**, the F-value for the selected model response is 28.50, and the corresponding p-value is <0.0001. As per Table 5, the notable terms of the model for electrochemical detection response for 3-MCPD are A, B, C, D, AB, BC, A2, B2, and C2. Thus, the second-order equation for the polynomial model between the investigated variables and the response sensitivity is shown in Eq. (2):

The equation (Eq.2) was used to calculate predicted response values. A positive sign for the regression model's coefficients denotes a synergistic effect, whereas a negative sign denotes an antagonistic impact on the response [39]. From Eq. (2), the constant 0.48 was not affected by any factor or correlation of factors, and the interaction terms A, B, C, D, A2, B2, and C2 had a negative effect on the response, showing that the sensitivity of 3-MCPD detection dropped when these terms were raised. Meanwhile, the terms AB and BC which are represented by the positive sign had a positive impact, indicating that as the magnitude of these terms increased, the sensitivity in 3-MCPD detection increased as well. The coefficient of determination (R^2) of 0.9814 and adjusted R^2 of 0.9470 are additional survey considerations and indicators of the validity of the selected polynomial model for the fitness of the data.

The experimental results were also assessed via diagnostic tools to validate the residuals' normality. The significance of the selected factors and the veracity of the assumptions are indicated by all the data points close to the linear line [40]. **Figure 3a** displays the conformity between the actual and expected data for the detection of 3-MCPD by MIPPy/CHT. The real value is determined by the data from each run of the experiment, whereas the predicted value is determined by the data obtained from the model using Design-Expert software (version 13, Stat-Ease, Minneapolis, USA). **Figure 3b** shows a dot diagram or a normal probability map of these residuals. Since most of the data points lean closely to the diagonal line, as seen from the plot (**Figure 3b**), a remarkable correlation between the actual and predicted values was found. **Figure 3c** shows that all the data are within the residual limits (±5.02973), demonstrating the validity of the model [41]. All these statistical experiments show that quadratic models corroborate well between independent factors and 3-MCPD detection response.

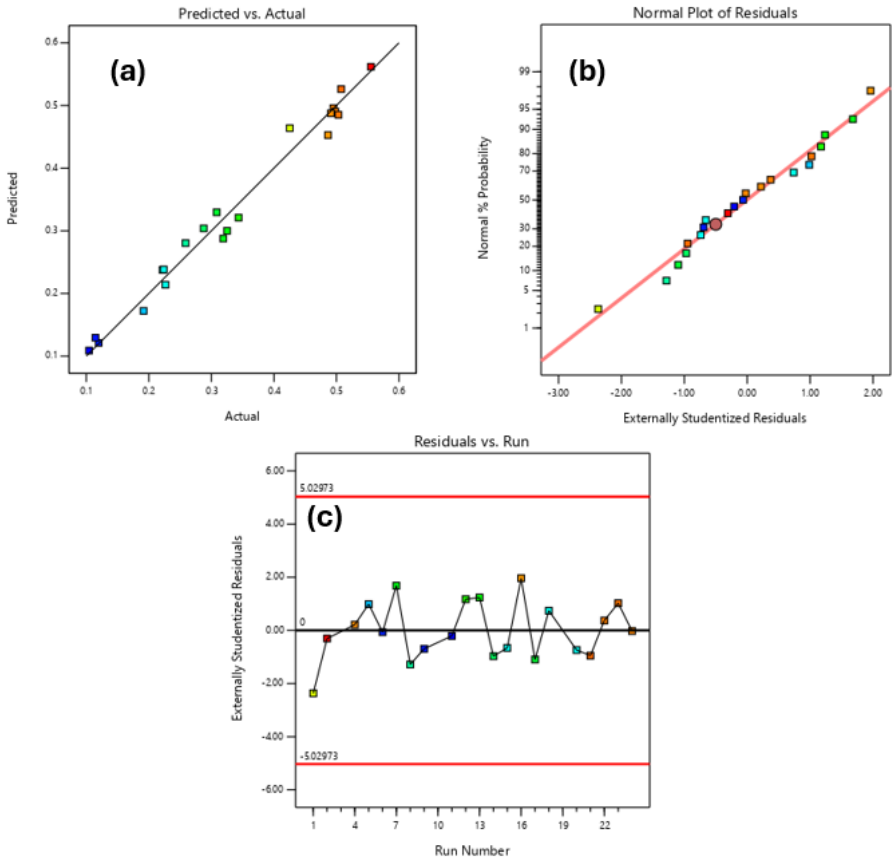


Figure 3. Plots of (a) actual vs predicted, (b) normal (%) probability of the residuals and (c) residual vs run

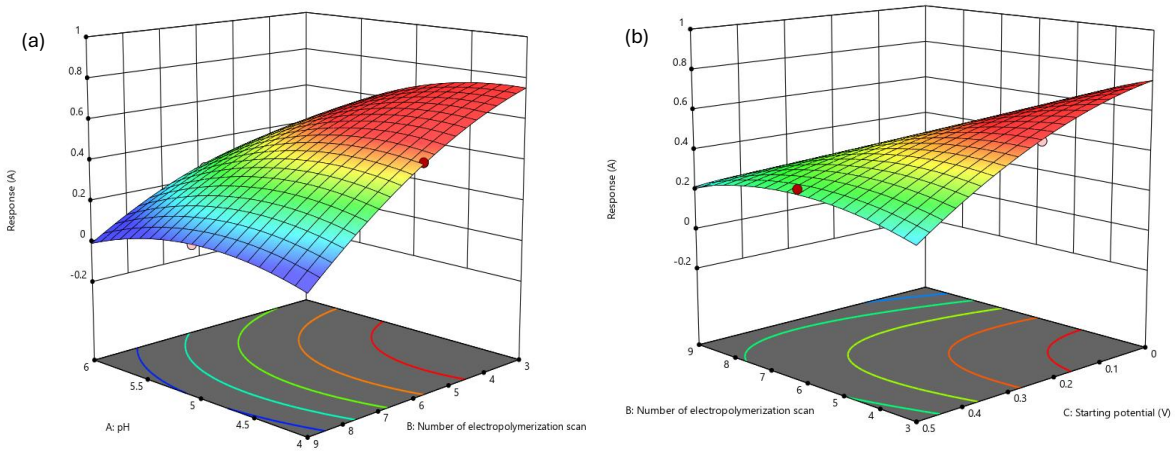


Figure 4. 3D plots of synergistic interactions (a) between (A) pH and (B) number of electropolymerization scan, and (B) number of electropolymerization and (C) starting potential

The three-dimensional (3D) response surface plots were built using Design-Expert software (version 13.0.5.0, 64 bit) by correlating two factors within the range and holding another factor at a specific level so that the correspondence between the response and the factors can be assessed. **Figure 4** presents the 3D response surface plots. The first significant interactive effect on the 3-MCPD detection, with a p-value of 0.0083, can be observed between A: pH and B: number of electropolymerization scans as illustrated in **Figure 4a**. This substantial interaction shows the crucial role of polymer-monomer interaction strength and imprinted polymer film layer. As shown in **Figure 4a**, by reducing the number of electropolymerization scans to 3 and decreasing the pH to 4, a significant increment in the response was observed in the detection of 3-MCPD from 0 to 0.75. At acidic pH, the functional monomer and 3-MCPD exhibit stronger hydrogen-bonding and electrostatic interactions, promoting the formation of well-defined and stable imprinted cavities. However, increasing the number of electropolymerization scans beyond the optimal level results in excessive polymer growth, leading to a thicker film that restricts mass transport and slows electron transfer kinetics. Therefore, although acidic conditions enhance binding affinity, excessive film thickness counteracts this benefit by increasing charge-transfer resistance, explaining the dome-shaped response surface and confirming the necessity of balancing chemical interaction strength with film thickness control.

The second significant interactive effect on the 3-MCPD detection with a p-value of 0.0001 can be observed between B: number of electropolymerization scans and C: starting potential of electropolymerization as illustrated in Figure 4b, where an increment from 0.2174 to 0.7523 occurs. The response surface indicates that optimal peak current is achieved at lower starting potentials combined with fewer number of scans. A lower starting potential promotes controlled nucleation and uniform polymer deposition. When coupled with a limited number of number of electropolymerization scans, this condition produces a thin, homogeneous MIP layer with accessible recognition sites and efficient electron transfer. In contrast, higher starting potentials and excessive number of scans accelerate polymerization, increasing crosslinking density and film thickness, which can partially insulate the electrode surface and hinder the elution of the 3-MCPD template during elution, thus potentially lowering the number of cavities. The curvature observed in the interaction plot confirms that both parameters jointly regulate the imprinted polymer, cavity accessibility, and charge-transfer efficiency, thereby critically influencing the sensitivity of 3-MCPD detection.

Figure 5 illustrates the response of solo factors for optimization of the electrochemical MIP sensor toward 3-MCPD detection. Each graph represents one-factor plots showing the individual effects of (A) pH, (B) number of electropolymerization scan, (C) starting potential, and (D) elution time on the peak current response. In these plots, the solid black line represents the predicted model response, dashed lines denote the confidence intervals, and the red markers indicate experimental design points. A pronounced negative curvature is observed for pH, scan number, and starting potential, indicating strong quadratic effects. Specifically, increasing pH from 4 to 6 results in a marked decrease in peak current, confirming that mildly acidic conditions favor stronger interaction between 3-MCPD and the functional monomer within the imprinted cavities. Similarly, increasing the number of electropolymerization scans leads to a reduction in response beyond the optimal level, suggesting that excessive film thickness hinders electron transfer and limits analyte diffusion. Starting potential also exhibits a significant non-linear influence, where higher starting potentials reduce sensor response due to difference in polymer growth kinetics and possible over-oxidation effects [42]. In contrast, elution time shows a relatively flatter profile within the investigated range, indicating a less pronounced but still relevant contribution once sufficient template removal is achieved.

The Box-Behnken design was used to systematically explore the effects of four factors (pH, elution time, potential range [starting potential], and Number of Scan) at three levels (low, medium, high). The experimental setup involved conducting a series of experiments where these factors were varied according to the Box-Behnken design principles. The following key findings were determined:

- Number of Scan (B): The optimal Number of Scan was determined to be 3. This value produced the best results, and both fewer and more scans showed a lower response during the detection of 3-MCPD.
- pH (A): The optimal pH value for the system's performance was found to be 4. This pH level led to the best output, while deviations from this value resulted in suboptimal performance.
- Starting potential (C): The potential range study showed that the greater the potential range (starting at 0V) during electropolymerization, the higher the MIP's stability.
- Elution Time (D): The optimal Elution Time was determined to be 15 minutes. This time maximized the system's efficiency, and shorter or longer elution times led to reduced performance.

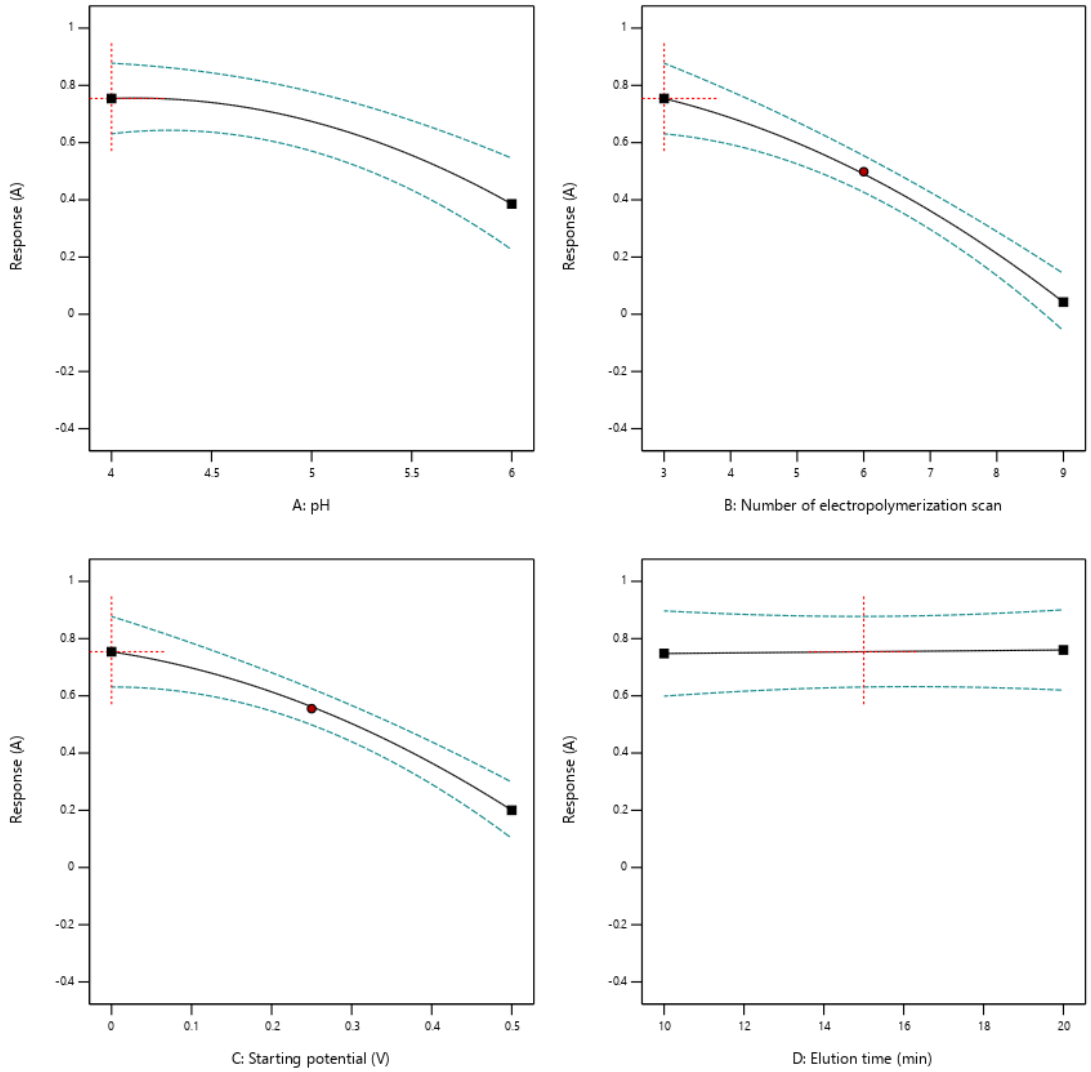


Figure 5. All-factor response chart of Box-Behnken experimental model

Characterisation of MIPPy/CHT

FESEM analysis

The bare SPCE surface (**Figure 6a**) exhibits a relatively compact morphology composed of closely packed carbon particles with particle sizes typically in the range of ~24–49 nm. The surface appears dense with limited porosity, providing a stable but non-selective conductive substrate. After electropolymerization (**Figure 6b**), the surface morphology becomes more heterogeneous, with increased particle agglomeration. The particle sizes are enlarged to approximately ~46–79 nm, indicating the successful formation of the MIP [43]. Following template removal (**Figure 6c**), the eluted MIP exhibits a noticeably more porous and loosely packed structure. The particle sizes are distributed in the range of ~31–70 nm, and the presence of nanoscale cavities is observed (indicated by yellow arrow in **Figure 6**). This increase in surface porosity and reduction in packing density is attributed to the extraction of 3-MCPD molecules. Upon rebinding with 3-MCPD (**Figure 6d**), the polymer surface becomes denser and more compact, with partial disappearance of the previously observed pores. The particle sizes are reduced and more uniformly distributed, typically in the range of ~40–67 nm. The decrease in porosity and increased packing density indicates effective rebinding of 3-MCPD molecules into the imprinted cavities. The obtained data agrees with several published reports [44-47].

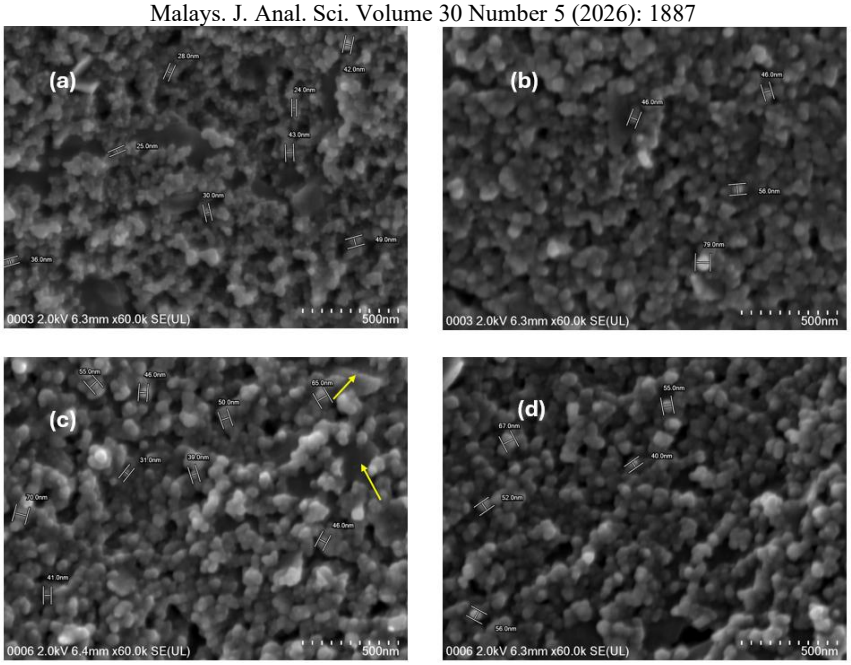


Figure 6. FESEM images of (a) SPCE, (b) MIPPy/CHT, (c) Eluted MIPPy/CHT, (d) and Rebound MIPPy/CHT

EDX analysis

The bar graph in **Figure 7** illustrates the chlorine content, expressed as weight percent (wt%), determined by Energy Dispersive X-ray Spectroscopy (EDX) for the Molecularly Imprinted Polymer (MIP), Eluted (MIP after removal), and Rebound MIP samples. The presence of chlorine (Cl) can be attributed to the target analyte, 3-MCPD. As shown in Scheme 1, the molecular structure of 3-MCPD contains a terminal chlorine atom, which contributes to the detected Cl signal. This is consistent with the molecular imprinting process, where the template molecule (3-MCPD) is embedded within the polymer matrix during fabrication. The MIP exhibited the highest chlorine content (~0.62 wt%), indicating effective imprinting and chlorine adsorption. Following elution, the chlorine signal significantly decreased (~0.16 wt%), confirming the removal of the bound analyte. Upon rebinding of analyte, the chlorine signal increased to ~0.50 Wt%, demonstrating the MIP's capability to re-capture the target molecule. These results support and compliment the selective recognition and rebinding functionality of the MIP system. The presented data is in agreement with several previos studies [48-50].

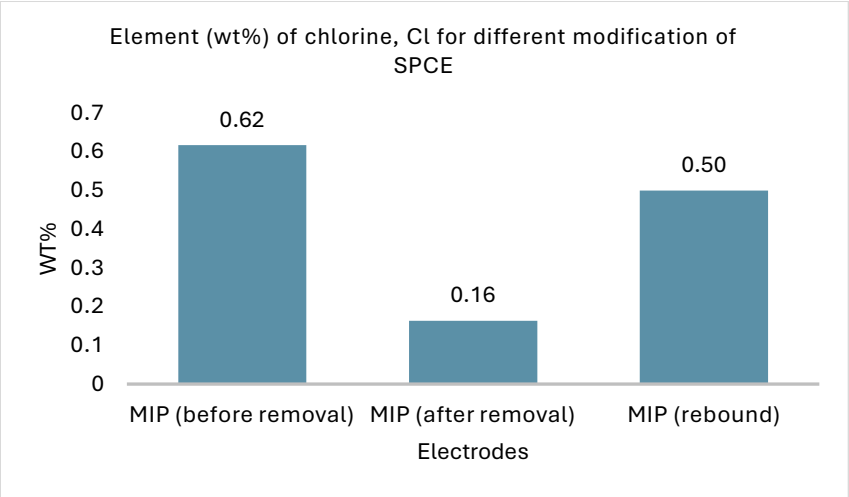
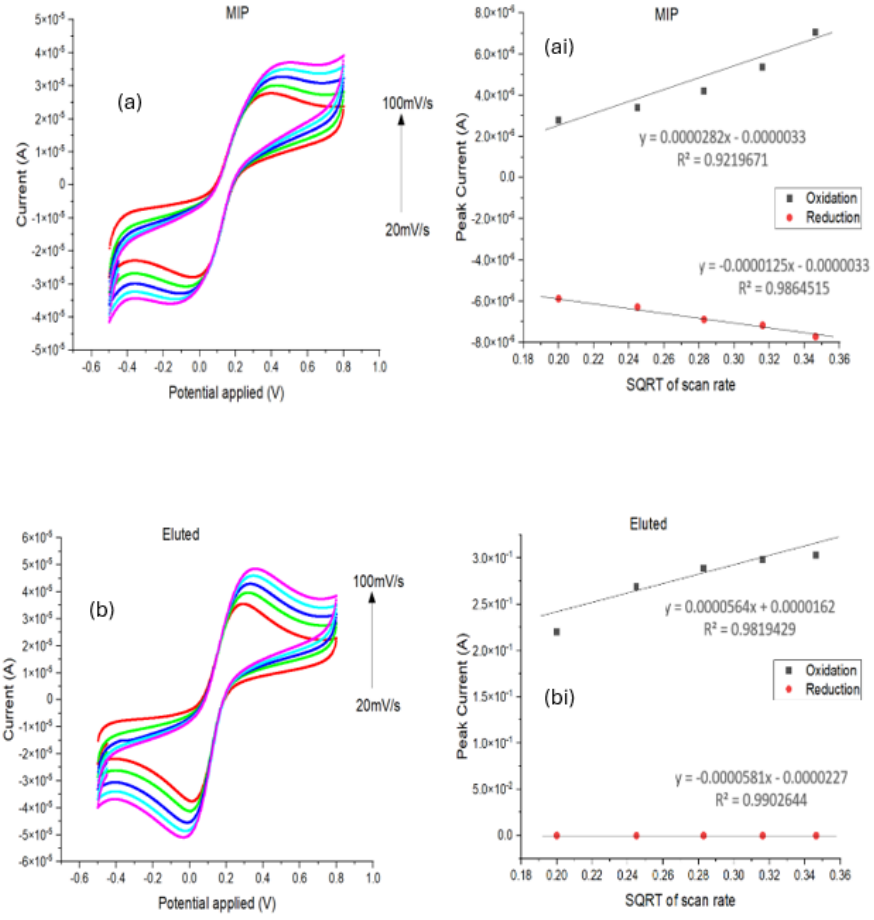


Figure 7. EDX analysis of chlorine for different stages of MIP sensor preparation and testing

Electroactive Surface Area (ECSA)

The electrochemical active surface area of the working electrode as shown in Figure 8 was evaluated by cyclic voltammetry (CV) using the equimolar $K_3[Fe(CN)_6]/K_4[Fe(CN)_6]$ prepared in 0.10 M KCl as the electrolyte. Cyclic voltammograms were recorded over a potential window spanning the $Fe(CN)_6^{3-}/Fe(CN)_6^{4-}$ redox couple (typically −0.5 to +0.80 V vs. Ag/AgCl) at scan rates ranging from 20 to 100 mV s^{-1}. Anodic and cathodic peak currents were extracted and plotted as a function of v^1/2, and the electroactive surface area was calculated from the slope using the Randles–Sevcik equation, employing a diffusion coefficient of 7.6×10^{-6} cm^2 s^{-1} for the ferro/ferricyanide electrolyte. The gradient obtained from the I_p vs. $v^{1/2}$ plots is directly proportional to the electrochemically active surface area (ECSA) according to the Randles–Sevcik equation [51].

The quantitative parameters derived from the Randles–Sevcik plots are summarized in **Table 6** with visual comparison using bar chart shown in **Figure 9**. The high correlation coefficients (R^2 = 0.986–0.999) confirm a strong linear dependence of peak current (I_p) on the square root of scan rate ($v^{1/2}$). The Bare electrode exhibited the highest gradient (2.1059×10^{-4}) and largest active area (5.79×10^{-5} cm^2), reflecting fast electron-transfer kinetics and unrestricted mass transport at the clean conductive interface. The Bare electrode exhibited the highest R^2 value (0.9993), indicating ideal diffusion behavior with minimal kinetic distortion, while slightly lower but still excellent R^2 values for the modified electrodes suggest minor interfacial resistance introduced by the polymer layers. Upon deposition of the MIP film, a significant decrease in gradient and ECSA (3.44×10^{-6} cm^2) was observed, which can be attributed to the insulating nature of the 3-MCPD molecule that partially blocks active sites and increases interfacial resistance. The NIP electrode showed an even lower active area (2.59×10^{-6} cm^2), suggesting a more compact and less porous polymer structure in the absence of template molecules, thereby further restricting electrolyte diffusion and electron transfer.



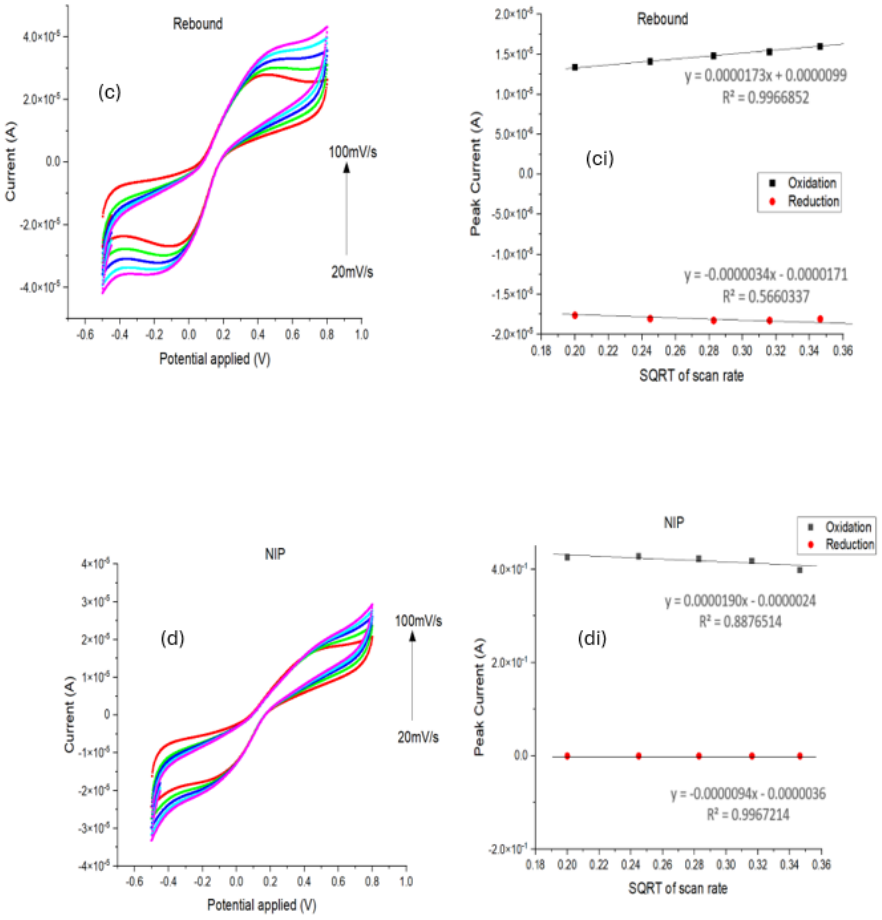


Figure 8. CV measurements on (a) MIPPy/CHT, (b) MIP-eluted, (c) MIP-rebound, (d) NIP with their respective Ip versus square root of scan rate plots (ai, bi, ci, di) for the anodic and cathodic currents in the 5 mM redox probe solution.

Table 6. Electrochemically active surface area for different electrodes

Electrode	R^2	Gradient	Area
Bare	0.999300243	0.00021059	5.79E-05
MIP	0.986451539	1.2507E-05	3.44E-06
NIP	0.996721414	9.423E-06	2.59E-06
Eluted	0.990264446	5.8119E-05	1.6E-05
Rebound	0.996685171	1.7288E-05	4.76E-06

Following template removal (Eluted), the gradient increased markedly, corresponding to a substantial rise in active area (1.60×10^{-5} cm²). This increment is due to the formation of cavities and porous channels, which improve electrolyte penetration, enlarge the effective contact area, and facilitate charge transport. Upon rebinding of analyte, the ECSA decreased again (4.76×10^{-6} cm²), consistent with occupation of these cavities by target molecules that hinder ion diffusion and partially block conductive pathways [52-56]. The overall trend as shown in Figure 9 (Bare > Eluted > Rebound > MIP > NIP) clearly demonstrates that the observed electrochemical changes arise from structural modifications at the electrode interface, providing strong evidence for successful imprint formation, cavity regeneration, and selective target recognition. The decrease in active area after polymer deposition confirms successful surface coverage, the increase after elution confirms cavity generation, and the decrease after rebinding verifies selective target capture. The

consistently high R^2 values further support that the observed differences arise from interfacial structural changes rather than kinetic artifacts. Collectively, these findings substantiate the effectiveness of the molecular imprinting strategy and demonstrate its direct influence on electrochemical surface properties.

Linear range and detection limit

The corresponding calibration curve shown in **Figure 10** (inset) exhibits a single linear region from the Δ signal (difference between rebound and eluted states) within (100–500 nM) concentration range, with a regression equation of Signal (A) = 0.00008[3-MCPD] + 0.4005 and an excellent correlation coefficient (R^2 = 0.9963), confirming the high linearity of the sensor response. As the analyte concentration changed from 100 to 500 nM, a systematic increase in Δ signal was observed, confirming concentration-dependent signal amplification. The comparative eluted and rebound profiles clearly reveal a pronounced decrease in current upon rebinding of analyte, verifying the successful formation of recognition cavities and selective re-occupation by 3-MCPD. The progressive amplification of the peak current difference with concentration indicates that more cavities are filled as the concentration increases, thus lowering the conductivity of the MIP sensor at higher concentrations [12, 57]. The limit of detection (LOD) and limit of quantitation (LOQ) were determined using a calibration-based approach (LOD = 3.3σ/slope), where σ represents the residual standard deviation of the regression ($S_{y/x}$), resulting in values of 36 nM and 111 nM, respectively. The quantitative measurements were restricted to the established linear range (100–500 nM), ensuring analytical reliability. Overall, the combination of stable peak potential, proportional signal amplification, high R^2 value, low regression variability, and statistically consistent detection limits collectively demonstrate that the developed electrochemical platform possesses strong analytical performance, high sensitivity, and reliable quantification capability for 3-MCPD detection.

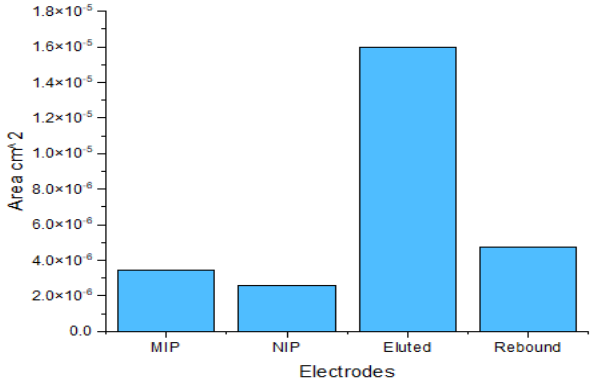


Figure 9. Bar chart of electroactive surface area of MIPPy/CHT, NIP MIP-eluted and MIP-rebound

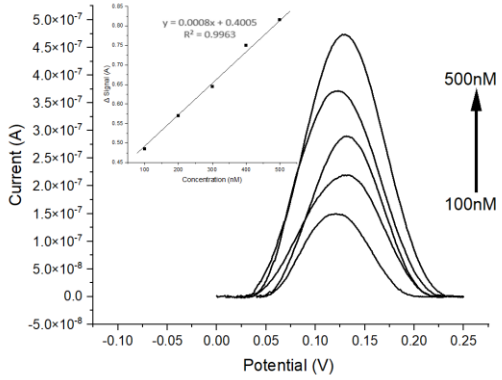


Figure 10. DPV curve shows the determination of 3-MCPD using MIPPy/CHT in the range of 100-500nM with the inset showing the calibration curve

The analytical performance of the proposed MIPPy/CHT-modified SPCE was evaluated in comparison with previously reported electrochemical sensors for 3-MCPD detection as shown in **Table 7**. Earlier studies employed diverse platforms including nanoparticle-modified gold electrodes, graphene oxide

composites, Prussian blue-deposited systems, MOF-integrated electrodes, and other molecularly imprinted polymer (MIP) configurations, many of which achieved very low limits of detection in the sub-nanomolar range. While these systems demonstrate excellent sensitivity, they frequently involve sophisticated nanomaterial synthesis, multi-step electrode modification, and relatively high fabrication costs. In addition, many of these reported systems rely on rigid electrode substrates such as glassy carbon or graphite, which are less suited for rapid, field-based deployment. In contrast, the present sensor provides a linear detection range of 100–500 nM with an LOD of 36 nM using a simple, cost-effective, and disposable SPCE platform. Although the sensitivity is comparatively moderate, it is sufficient for determining 3-MCPD in real food matrices such as soy sauce and cooking oil as regulatory limits established by the European Commission set a maximum level of 20 µg/kg for 3-MCPD in soy sauce and acid-hydrolyzed vegetable protein. While glassy carbon electrodes and graphite rods provide excellent performance in research, their reliance on bulky electrochemical cells and labor-intensive polishing protocols largely restricts them to a laboratory environment. SPCEs on the other hand offer a more practical alternative for field-based applications by integrating all three electrodes onto a single, compact substrate. The disposable nature of SPCEs eliminates the need for surface maintenance and prevents cross-contamination between tests. As they require only small (2-3 mililitre) sample volumes and can be used with portable, handheld potentiostats, SPCEs are better suited for on-site monitoring than traditional solid electrodes. Compared to MIP-based systems such as MIP/cMWCNT/MOF-199/GCE [60] and MIP/NPG/GCE [10], which can achieve lower LODs but require complex material integration, the present approach offers a simpler fabrication strategy with fewer modification steps while still maintaining adequate analytical performance. Importantly, the incorporation of molecular imprinting polymer enhances selectivity and matrix tolerance, offering a practical balance between sensitivity, simplicity, reproducibility, and on-site applicability. Overall, this comparison highlights that the proposed sensor prioritizes operational simplicity and applicability over extreme sensitivity, positioning it as a viable alternative for routine and field-based 3-MCPD monitoring.

Table 7. Comparison of the developed 3-MCPD sensor with other similar reported sensors

Material	Method	Linear Range nM	LOD (nM)	Matrix	Ref
Anodic alumina oxide nanotubes membrane	Direct GC–MS analysis	9.047-10856	0.6514	Vegetable oil	[58]
p-Aminothiophenol (p-ATP) on gold nanoparticle-modified glassy carbon electrode	CV/DPV	Log (1.0×10^{-6}-1.0×10^{-4})	3.8×10^{-9}	Soy sauce	[8]
Pt@PB (Prussian Blue)/EM-GP modified graphite paper (EM-GP)	CV/DPV	10 -50000	5	Palm, Peanut, Soybean oil	[11]
Polymer of p-amino thiophenol on gold nanoparticle graphite pencil electrode	EIS	1085.6-10042	1085.6	Cooking oil	[59]
Polypyrrole MIP (oPPy) on graphene oxide	EIS	2 -500	1.82	Soy sauce	[12]
MIP/cMWCNT/MOF-199/GCE	DPV	1-10000	0.43	Soy sauce	[60]
Cys-AgNPs/Au	CV/DPV	0.276-22.1078	0.2652	Palm oil and smoked mackerel	[61]
MIP/NPG/GCE	DPV	Log (10^{-7}-10^{2})	3.5×10^{-8}	Soy sauce	[10]
molecularly imprinted polymers/carbon dots-grafted paper	Fluorescence	0.110539 -16.58	0.06	Soy sauce	[18]
MIPPy/CHT on SPCE	DPV	100–500	36	Soy sauce and cooking oil	This work

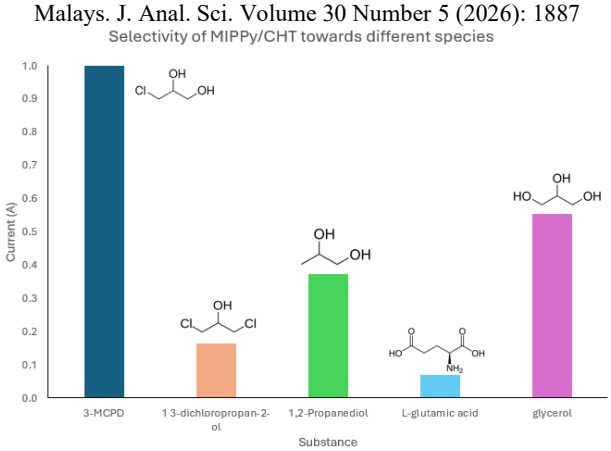


Figure 11. Selectivity of MIPPy/CHT sensor toward 3-MCPD in comparison with structurally related and potentially interfering substances

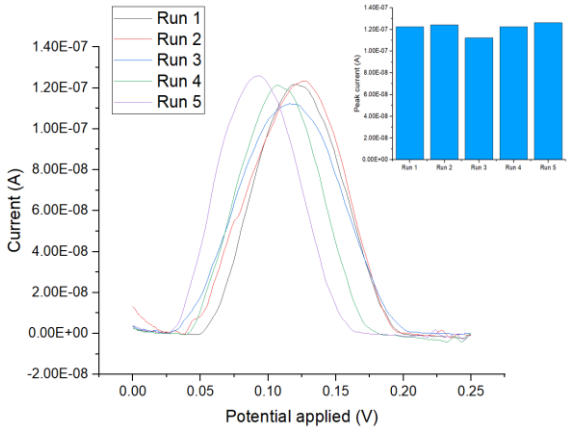


Figure 12. Voltammetric responses from five consecutive runs of MIPPy/CHT sensor toward 3-MCPD

Selectivity studies

The bar graph in **Figure 11** presents the peak current responses of the MIPPy/CHT-modified electrode toward 3-MCPD and other structurally related compounds, namely L-glutamic acid, 1,3-dichloropropan-2-ol, 1,2-propanediol, and glycerol. Among the tested substances, 3-MCPD exhibits a normalized response of 1.0, confirming that it generates the maximum electrochemical signal due to optimal rebinding within the molecularly imprinted cavities. This strong response reflects high structural complementarity between the imprinted recognition sites and the template molecule owing to appropriate cavity size, geometry, and functional group orientation that promote effective hydrogen bonding and specific interactions. In contrast, the response to L-glutamic acid and 1,3-dichloropropan-2-ol was significantly lower (0.0686 A and 0.1646 A, respectively), indicating minimal non-specific binding. Moderate signals were observed for 1,2-propanediol (0.373 A) and glycerol (0.555 A), which are both structurally similar to 3-MCPD, but lacking the complete imprint complementarity. These results highlight the high selectivity of the MIPPy/CHT system for 3-MCPD, confirming its suitability for targeted sensing applications in complex matrices. Overall, the pronounced signal difference between 3-MCPD and other tested species confirms the high selectivity of the MIPPy/CHT sensor. The normalized presentation clearly demonstrates that the sensor response is dominantly governed by template-specific recognition rather than non-specific adsorption, validating the effectiveness of the molecular imprinting strategy for selective 3-MCPD detection in complex sample matrices.

Reproducibility

The voltametric responses obtained from five consecutive runs exhibit closely overlapping peak shapes and positions, indicating good repeatability of the electrochemical measurement. As shown in the **Figure 12**, all runs display a well-defined anodic peak within a narrow potential window (~0.10–0.14 V), with only

Table 8. Determination of 3-MCPD using the MIPPy/CHT sensor in the soy sauce and palm oil sample

Matrix (n=3)	Spiked	Recovered	Recovery %	RSD
Soy sauce	150nM	158.1638	99.0495	0.004654
Palm oil	250nM	226.0957	96.94628	0.005425

minor variations in peak height and slight shifts in peak potential. This consistency is also reflected in the inset bar chart, where the peak currents fall within a narrow range (1.34×10^{-7} to 1.40×10^{-7} A). The relative standard deviation (RSD) of the peak current measurements was calculated to be 1.67%, indicating very low variability between the five runs.

Real sample analysis

The applicability of the proposed MIPPy/CHT/SPCE sensor was evaluated through recovery experiments shown in **Table 8** in both soy sauce and palm oil using the standard addition method [62-64]. The recoveries obtained were 99.05% for soy sauce (150 nM spike) and 96.95% for palm oil (250 nM spike). The relative standard deviation (RSD) values were below 0.006, indicating good repeatability of the measurements. The recovery values close to 100% suggest that matrix components such as salts in soy sauce and lipids in palm oil did not significantly interfere with the detection of 3-MCPD. These results confirm that the molecularly imprinted sensor can accurately quantify 3-MCPD in complex food matrices with satisfactory precision, supporting its suitability for routine analysis of real samples.

Conclusion

In this study, a molecularly imprinted polypyrrole/chitosan based electrochemical sensor was successfully developed and optimized for the selective detection of 3-monochloropropane-1,2-diol. A systematic optimization strategy was implemented using response surface methodology, where a two-level factorial design was first employed to evaluate critical fabrication parameters, including pH, number of electropolymerization scans, starting potential, and elution time. Statistical analysis (ANOVA) confirmed the significant influence of these factors, with pronounced quadratic effects observed for pH, scan number, and starting potential. Further optimization using a Box–Behnken design established optimal conditions at pH 4, 3 number of scans, controlled starting potential, and 15 minutes elution time, emphasizing the importance of balancing polymer thickness, cavity accessibility, and charge-transfer efficiency. The electrochemically active surface area analysis revealed significant differences among the electrode configurations, where the surface area decreases (Eluted > Rebound > MIP) further support the effectiveness of template(3-MCPD) removal and analyte(3-MCPD) detection of the sensor. The optimized sensor demonstrated excellent analytical performance, exhibiting a linear response over the concentration range of 100–500 nM with a high correlation coefficient ($R^2 = 0.9963$) and a low detection limit of 36 nM. The proportional increase in Δcurrent with concentration confirms effective and selective rebinding within the imprinted cavities. Additionally, the sensor showed good reproducibility and high selectivity toward 3-MCPD.

Acknowledgement

Authors would like to show high gratitude to US-ASEAN – Science, Technology, and Innovation Cooperation Program from Arizona State University [100-TNCPI/INT 16/6/2 (047/2023)], Malaysia Toray Science Foundation [File No. 240529STRG0212], and Sensor Malaysia-Biogenes (SBRF) [100-TNCPI/PRI 16/6/2 (018/2024)] for the financial support provided to complete this research work.

References

1. Sulin, S., Mokhtar, M., Mohammed, M., & Baharuddin, A. (2020). Review on palm oil contaminants related to 3-monochloropropane-1, 2-diol (3-MCPD) and glycidyl esters (GE). *Food Research*, 4(S6), 11-18.
2. Buhrke, T., Schultrich, K., Braeuning, A., & Lampen, A. (2017). Comparative analysis of transcriptomic responses to repeated-dose exposure to 2-MCPD and 3-MCPD in rat kidney, liver and testis. *Food and Chemical Toxicology*, 106, 36-46.
3. Eisenreich, A., Monien, B. H., Götz, M. E., Buhrke, T., Oberemm, A., Schultrich, K., Abraham, K., Braeuning, A., & Schäfer, B. (2023). 3-MCPD as contaminant in processed foods: State of knowledge and remaining challenges. *Food Chemistry*, 403, 134332.
4. Chain, E. Panel o. C. i. t. F. (2016). Risks for human health related to the presence of 3- and 2-monochloropropanediol (MCPD), and their fatty acid esters, and glycidyl fatty acid esters in food. *EFSA Journal*, 14(5), e04426.
5. Wong, K. O., Cheong, Y. H., & Seah, H. L. (2006). 3-Monochloropropane-1,2-diol (3-MCPD) in soy and oyster sauces: Occurrence and dietary intake assessment. *Food Control*, 17(5), 408-413.

6. Baer, I., De la Calle, B., & Taylor, P. (2010). 3-MCPD in food other than soy sauce or hydrolysed vegetable protein (HVP). *Analytical and Bioanalytical Chemistry*, 396(1), 443-456.
7. Parisi, O. I., Francomano, F., Dattilo, M., Patitucci, F., Prete, S., Amone, F., & Puoci, F. (2022). The Evolution of Molecular Recognition: From Antibodies to Molecularly Imprinted Polymers (MIPs) as Artificial Counterpart. *Journal of Functional Biomaterials*, 13(1), 12. 2079-4983.
8. Sun, X., Zhang, L., Zhang, H., Qian, H., Zhang, Y., Tang, L., & Li, Z. (2014). Development and application of 3-chloro-1,2-propandiol electrochemical sensor based on a polyaminothiophenol modified molecularly imprinted film. *Journal of Agricultural and Food Chemistry*, 62(20), 4552-4557.
9. Martin, A. A., Fodjo, E. K., Eric-Simon, Z. V., Gu, Z., Yang, G., Albert, T., Kong, C., & Wang, H.-F. (2021). Cys-AgNPs modified gold electrode as an ultrasensitive electrochemical sensor for the detection of 3-chloropropane-1,2-diol. *Arabian Journal of Chemistry*, 14(9), 103319.
10. Cheng, W., Zhang, Q., Wu, D., Yang, Y., Zhang, Y., & Tang, X. (2022). A facile electrochemical method for rapid determination of 3-chloropropane-1,2-diol in soy sauce based on nanoporous gold capped with molecularly imprinted polymer. *Food Control*, 134, 108750.
11. Chi, H., Li, Y., & Liu, G. (2022). Molecularly imprinted sensing platform based on electrochemically modified graphite paper for efficient detection of 3-monochloropropane-1,2-diol. *Food Chemistry*, 386, 132829.
12. Yaman, Y. T., Bolat, G., Saygin, T. B., & Abaci, S. (2021). Molecularly imprinted label-free sensor platform for impedimetric detection of 3-monochloropropane-1,2-diol. *Sensors and Actuators B: Chemical*, 328, 128986.
13. Pang, A. L., Arsad, A., & Ahmadipour, M. (2021). Synthesis and factor affecting on the conductivity of polypyrrole: a short review. *Polymers for Advanced Technologies*, 32(4), 1428-1454.
14. Deng, F., Li, Y., Luo, X., Yang, L., & Tu, X. (2012). Preparation of conductive polypyrrole/TiO2 nanocomposite via surface molecular imprinting technique and its photocatalytic activity under simulated solar light irradiation. *Colloids and Surfaces A: Physicochemical and Engineering Aspects*, *395*, 183-189.
15. Xu, L., Huang, Y.-A., Zhu, Q.-J., & Ye, C. (2015). Chitosan in Molecularly-Imprinted Polymers: Current and Future Prospects. *International Journal of Molecular Sciences*, 16(8), 18328-18347.
16. Sambasevam, K. P., Sateria, S. F., Baharin, S. N. A., Azman, N. J., Ahmad Wakid, S., & Shahabuddin, S. (2023). An optimization of fungal chitin grafted polyaniline for ammonia gas detection via Box Behnken design. *International Journal of Biological Macromolecules*, 238, 124079.
17. Ferreira, S. L. C., Bruns, R. E., Ferreira, H. S., Matos, G. D., David, J. M., Brandão, G. C., da Silva, E. G. P., Portugal, L. A., dos Reis, P. S., Souza, A. S., & dos Santos, W. N. L. (2007). Box-Behnken design: An alternative for the optimization of analytical methods. *Analytica Chimica Acta*, *597*(2), 179-186.
18. Fang, M., Zhou, L., Zhang, H., Liu, L., & Gong, Z.-Y. (2019). A molecularly imprinted polymers/carbon dots-grafted paper sensor for 3-monochloropropane-1,2-diol determination. *Food Chemistry*, 274, 156-161.
19. Xing, X., & Cao, Y. (2007). Determination of 3-chloro-1,2-propanediol in soy sauces by capillary electrophoresis with electrochemical detection. *Food Control*, 18(2), 167-172.
20. Geng, X., Kwon, O.-H., & Jang, J. (2005). Electrospinning of chitosan dissolved in concentrated acetic acid solution. *Biomaterials*, *26*(27), 5427-5432.
21. Albar, M. M. J., Jamion, N. A., Baharin, S. N. A., Raoov, M., & Sambasevam, K. P. (2020). Preparation of novel commercial polyaniline composites for ammonia detection. *Solid State Phenomena,* 301, 124-131.
22. Yang, Y., Fang, G., Wang, X., Pan, M., Qian, H., Liu, H., & Wang, S. (2014). Sensitive and selective electrochemical determination of quinoxaline-2-carboxylic acid based on bilayer of novel poly(pyrrole) functional composite using one-step electro-polymerization and molecularly imprinted poly(o-phenylenediamine). *Analytica Chimica Acta*, 806, 136-143.
23. Bougrini, M., Florea, A., Cristea, C., Sandulescu, R., Vocanson, F., Errachid, A., Bouchikhi, B., El Bari, N., & Jaffrezic-Renault, N. (2016). Development of a novel sensitive molecularly imprinted polymer sensor based on electropolymerization of a microporous-metal-organic framework for tetracycline detection in honey. *Food Control*, *59*, 424-429.
24. Pfaff, T. J. (2023). Formulas Quantifying Change. In T. J. Pfaff (Ed.), *Applied Calculus with R* (pp. 65-76). Springer International Publishing.
25. Ahmed, R. K., Saad, E. M., Fahmy, H. M., & El Nashar, R. M. (2022). Multivariate experimental

design: towards more reliable electrochemical detection. *Current Opinion in Electrochemistry*, 31, 100880.

26. Ling, T.-R., Hsieh, W.-C., Li, Y.-Y., & Hung, T.-T. (2023). MIP sensor made using multi-current step electro-polymerization method on framed Ag-SPE for glutamic acid enantiomer recognition. *Journal of Electroanalytical Chemistry*, 944, 117635.
27. Zembrzuska, D., Kalecki, J., Cieplak, M., Lisowski, W., Borowicz, P., Noworyta, K., & Sharma, P. S. (2019). Electrochemically initiated co-polymerization of monomers of different oxidation potentials for molecular imprinting of electroactive analyte. *Sensors and Actuators B: Chemical*, 298, 126884.
28. Wu, Y., Li, G., Tian, Y., Feng, J., Xiao, J., Liu, J., Liu, X., & He, Q. (2021). Electropolymerization of molecularly imprinted polypyrrole film on multiwalled carbon nanotube surface for highly selective and stable determination of carcinogenic amaranth. *Journal of Electroanalytical Chemistry*, 895, 115494.
29. Di Masi, S., De Benedetto, G. E., & Malitesta, C. (2024). Optimisation of electrochemical sensors based on molecularly imprinted polymers: from OFAT to machine learning. *Analytical and Bioanalytical Chemistry*, 416(9), 2261-2275.
30. Szpisják-Gulyás, N., Al-Tayawi, A. N., Horváth, Z. H., László, Z., Kertész, S., & Hodúr, C. (2023). Methods for experimental design, central composite design and the Box–Behnken design, to optimise operational parameters: A review. *Acta Alimentaria*, *52*(4), 521-537.
31. Martin, A. A., Fodjo, E. K., Marc, G. B. I., Albert, T., & Kong, C. (2021). Simple and rapid detection of free 3-monochloropropane-1,2-diol based on cysteine modified silver nanoparticles. *Food Chemistry,* 338, 127787.
32. Alizadeh, T., Ganjali, M. R., Zare, M., & Norouzi, P. (2010). Development of a voltammetric sensor based on a molecularly imprinted polymer (MIP) for caffeine measurement. *Electrochimica Acta*, *55*(5), 1568-1574.
33. da Silva, H., Pacheco, J., Silva, J., Viswanathan, S., & Delerue-Matos, C. (2015). Molecularly imprinted sensor for voltammetric detection of norfloxacin. *Sensors and Actuators B: Chemical*, 219, 301-307.
34. Cheng, Z., Wang, E., & Yang, X. (2001). Capacitive detection of glucose using molecularly imprinted polymers. *Biosensors and Bioelectronics*, 16(3), 179-185.
35. Akpinar, H., Nurioglu, A. G., & Toppare, L. (2012). Influence of hydrogen bonding on electrochromic properties of conducting polymers. *Journal of Electroanalytical Chemistry*, 683, 62-69.
36. Yang, R., Ruan, C., Dai, W., Deng, J., & Kong, J. (1999). Electropolymerization of thionine in neutral aqueous media and H_2O_2 biosensor based on poly(thionine). *Electrochimica Acta*, 44(10), 1585-1596.
37. Tamandani, M., & Hashemi, S. H. (2022). Central Composite Design (CCD) and Box-Behnken Design (BBD) for the Optimization of a Molecularly Imprinted Polymer (MIP) Based Pipette Tip Micro-Solid Phase Extraction (SPE) for the Spectrophotometric Determination of Chlorpyrifos in Food and Juice. *Analytical Letters*, 55(15), 2394-2408.
38. Sulaiman, N. S., Hashim, R., Mohamad Amini, M. H., Danish, M., & Sulaiman, O. (2018). Optimization of activated carbon preparation from cassava stem using response surface methodology on surface area and yield. *Journal of Cleaner Production*, 198, 1422-1430.
39. Das, S., & Mishra, S. (2017). Box-Behnken statistical design to optimize preparation of activated carbon from *Limonia acidissima* shell with desirability approach. *Journal of Environmental Chemical Engineering*, *5*(1), 588-600.
40. Natarajan, E., & Ponnaiah, G. P. (2017). Optimization of process parameters for the decolorization of Reactive Blue 235 dye by barium alginate immobilized iron nanoparticles synthesized from aluminum industry waste. *Environmental Nanotechnology, Monitoring & Management*, *7*, 73-88.
41. Ghoreishian, S. M., Raju, G. S. R., Pavitra, E., Kwak, C. H., Han, Y.-K., & Huh, Y. S. (2019). Ultrasound-assisted heterogeneous degradation of tetracycline over flower-like rGO/CdWO4 hierarchical structures as robust solar-light-responsive photocatalysts: Optimization, kinetics, and mechanism. *Applied Surface Science*, 489, 110-122.
42. Ozkorucuklu, S. P., Sahin, Y., & Alsancak, G. (2008). Voltammetric behaviour of sulfamethoxazole on electropolymerized-molecularly imprinted overoxidized polypyrrole. *Sensors*, 8(12), 8463-8478.
43. Zeb, S., Wong, A., Khan, S., Hussain, S., & Sotomayor, M. D. P. T. (2021). Using magnetic nanoparticles/MIP-based electrochemical sensor for quantification of tetracycline in milk samples. *Journal of Electroanalytical Chemistry*, 900, 115713.

44. Naskar, H., Ghatak, B., Biswas, S., Singh, P. P., Tudu, B., & Bandyopadhyay, R. (2020). Electrochemical detection of eugenol (EU) using polyacrylonitrile molecular imprinted polymer embedded graphite (PAN-MIP/G) electrode. *IEEE Sensors Journal*, 20(1), 39-46.
45. Chatterjee, T. N., Das, D., Roy, R. B., Tudu, B., Sabhapondit, S., Tamuly, P., Pramanik, P., & Bandyopadhyay, R. (2018). Molecular imprinted polymer based electrode for sensing catechin (+C) in green tea. *IEEE Sensors Journal*, 18(6), 2236-2244.
46. Yang, S., Wang, Y., Xu, M., He, M., Zhang, M., Ran, D., & Jia, X. (2013). Synthesis of modified chitosan-based molecularly imprinted polymers for adsorptive protein separation. *Analytical Methods*, 5(20), 5471-5477.
47. Khoo, W. C., Kamaruzaman, S., Lim, H. N., Jamil, S. N. A. M., & Yahaya, N. (2019). Synthesis and characterization of graphene oxide-molecularly imprinted polymer for Neopterin adsorption study. *Journal of Polymer Research*, 26(8), 184.
48. Saidin, M. I., Sidik, S. M., & Ul-Hamid, A. (2024). Nickel-Zinc supported on mesoporous silica nanoparticles and its potential as a paracetamol sensor. *Journal of Smart Sensors and Materials*, *2*(1), 4.
49. Prabhu, S. N., Mukhopadhyay, S. C., Gooneratne, C. P., Davidson, A. S., & Liu, G. (2020). Molecularly imprinted polymer-based detection of creatinine towards smart sensing. *Medical Devices & Sensors*, *3*(6), e10133.
50. Prabhu, S. N., Gooneratne, C. P., & Mukhopadhyay, S. C. (2021). Development of MEMS sensor for detection of creatinine using MIP based approach – a tutorial paper. *IEEE Sensors Journal*, *21*(20), 22170-22181.
51. Mundinamani, S., & Rabinal, M. K. (2014). Cyclic voltammetric studies on the role of electrode, electrode surface modification and electrolyte solution of an electrochemical cell. *IOSR Journal of Applied Chemistry*, *7*, 45-52.
52. Lin, R., Huang, P., Ségalini, J., Largeot, C., Taberna, P. L., Chmiola, J., Gogotsi, Y., & Simon, P. (2009). Solvent effect on the ion adsorption from ionic liquid electrolyte into sub-nanometer carbon pores. *Electrochimica Acta*, *54*(27), 7025-7032.
53. Said, N. A. M., Awaludin, N., Salam, F., Razali, H., Ghazali, M. S., Talib, M. A. A., ... & Misman, S. N. (2023). Carboxylated multi-walled carbon nanotubes modified screen-printed electrodes for early detection of rice diseases using immunosensor approach. *Journal of Smart Sensors and Materials*, 1(1), 59-74.
54. Salinas-Torres, D., Huerta, F., Montilla, F., & Morallón, E. (2011). Study on electroactive and electrocatalytic surfaces of single walled carbon nanotube-modified electrodes. *Electrochimica Acta*, 56(5), 2464-2470.
55. Ahmad, K., Kumar, P., & Mobin, S. M. (2020). A highly sensitive and selective hydroquinone sensor based on a newly designed N-rGO/$SrZrO_3$ composite. *Nanoscale Advances*, *2*(1), 502-511.
56. Singh, R. K., & Schechter, A. (2018). Electrochemical investigation of urea oxidation reaction on β $Ni(OH)_2$ and $Ni/Ni(OH)_2$. *Electrochimica Acta*, 278, 405-411.
57. Sambasevam, K. P., Baharin, S. N. A., Zulkifli, A., Raoov, M., Asman, S., Mohamed, A. H., & Marimuthu, T. (2025). Factorial design assisted electrochemical detection of cypermethrin using molecularly imprinted polyaniline. *Pure and Applied Chemistry*, 97(8), 865-882.
58. Qiu, X., Xu, X.-Y., Liang, Y., & Guo, H. (2018). The molecularly imprinted polymer supported by anodic alumina oxide nanotubes membrane for efficient recognition of chloropropanols in vegetable oils. *Food Chemistry*, 258, 295-300.
59. Banurea, I. R., Sanjaya, A. R., Nizardo, N. M., & Ivandini, T. A. (2023). Molecularly imprinted polymer of p-amino thiophenol for a 3-monochloropropane-1,2-diol impedance-based sensor. *Materials Chemistry and Physics*, 301, 127613.
60. Han, S., Ding, Y., Teng, F., Yao, A., & Leng, Q. (2021). Determination of chloropropanol with an imprinted electrochemical sensor based on multi-walled carbon nanotubes/metal–organic framework composites. *RSC Advances*, 11(30), 18468-18475.
61. Martin, A. A., Fodjo, E. K., Eric-Simon, Z. V., Gu, Z., Yang, G., Albert, T., Kong, C., & Wang, H.-F. (2021). Cys-AgNPs modified gold electrode as an ultrasensitive electrochemical sensor for the detection of 3-chloropropane-1, 2-diol. *Arabian Journal of Chemistry*, 14(9), 103319.
62. Rodríguez, L. C., Campaña, A. G., Barrero, F. A., Linares, C. J., & Ceba, M. R. (1995). Validation of an analytical instrumental method by standard addition methodology. *Journal of AOAC International*, 78(2), 471-476.
63. Sambasevam, K. P., Mohamad, S., & Phang, S-W. (2017). Chemical sensor for hydrazine detection using polyaniline thin film. *Malaysian Journal of Analytical Sciences,* 21(4), 762-769.
64. Saxberg, B. E., & Kowalski, B. R. (1979). Generalized standard addition method. *Analytical Chemistry*, *51*(7), 1031-1038.